

Text-Driven 3D Indoor Scene Synthesis in Non-Manhattan Environments

Xianhui Meng^{1,2}, Zirui Song^{2,3}, Yuchen Zhang^{2,4}, Li Zhang¹,
Yongxuan Lv¹, Xiuying Chen³, Kun Wang⁵, Yan Luo⁶, Kai Chen⁷, Hangjun Ye²,
Long Chen², Jun Liu^{1*}, Xiaoshuai Hao^{2*},

¹University of Science and Technology of China, ²Xiaomi EV,

³Mohamed bin Zayed University of Artificial Intelligence, ⁴Georgia Institute of Technology,

⁵Nanyang Technological University, ⁶Massachusetts Institute of Technology,

⁷The Hong Kong University of Science and Technology,

junliu@ustc.edu.cn, haoxiaoshuai@xiaomi.com

Abstract

Large Language Models (LLMs) have demonstrated remarkable capabilities in 3D indoor scene synthesis for Manhattan environments. However, existing methods often fail to capture plausible object layout patterns in non-Manhattan settings, primarily because they struggle to model non-orthogonal spatial relationships, leading to high geometric violations and low physical fidelity. To address this challenge, we propose *SPG-Layout*, a novel text-driven framework designed to generate physically plausible indoor scenes within complex non-Manhattan environments. Specifically, we first utilize *statistical priors* of object distributions to guide the training process, enhancing environmental understanding and fidelity. Furthermore, mirroring human design workflows, we adopt a *hierarchical layout strategy* that prioritizes the placement of large objects, thereby substantially minimizing layout violations. By synergizing these components, *SPG-Layout* achieves a balanced optimization of semantic realism and physical plausibility. To evaluate performance in these complex settings, we constructed a new benchmark comprising 500 diverse non-Manhattan environments. Extensive experiments demonstrate that *SPG-Layout* consistently and significantly outperforms existing methods across both Manhattan and non-Manhattan environments. The code will be publicly released.

1 Introduction

Recent advancements in Large Language Models (LLMs) have revolutionized text-driven 3D scene synthesis, enabling users to generate complex environments using natural language (Bucher and Armeni 2025; Yang et al. 2024d; Tang et al. 2024; Hu et al. 2024a; Maillard et al. 2024; Sun et al. 2024a; Feng et al. 2023; Hao et al. 2025). However, a critical disparity remains between academic benchmarks and real-world architectural complexity. The vast majority of existing methods predominantly focus on Manhattan environments, characterized by simplified layouts with orthogonal walls and axis-aligned structures. While the *Manhattan Assumption* facilitates grid-based generation, it significantly limits applicability in practical scenarios. In real-world indoor scenes, non-Manhattan topologies are not merely edge cases but are,

*Corresponding author.

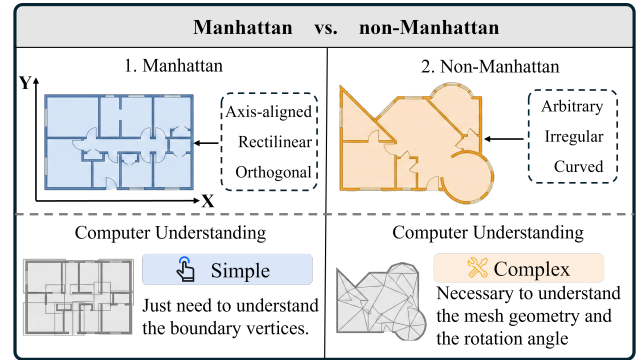


Figure 1: **Manhattan vs. Non-Manhattan Environments.** Manhattan environments (left) are simple, characterized by orthogonal structures. In contrast, non-Manhattan environments (right) are difficult to understand due to their arbitrary, irregular, and curved geometries, requiring precise reasoning about mesh details and rotation angles.

in fact, prevalent. Contemporary architecture frequently employs complex geometric primitives, characterized by arbitrary turning angles, curvilinear boundaries, and irregular polygons, as illustrated in Fig. 1.

However, extending current generative paradigms to non-Manhattan settings presents non-trivial challenges. First, existing approaches (Bucher and Armeni 2025; Song et al. 2025; Yang et al. 2024d; Wang et al. 2023; Zhai et al. 2024; Lin and Mu 2024; Sun et al. 2024b; Feng et al. 2023, 2025) learned distributions implicitly assume axis-aligned boundaries, so high-likelihood placements in Manhattan rooms may become physically infeasible once walls turn obliquely. Second, existing methods (Çelen et al. 2024; Fu et al. 2024; Hu et al. 2024b; Littlefair, Dutt, and Mitra 2025; Yang et al. 2024c; Wang et al. 2024; Aguina-Kang et al. 2024; Xia et al. 2025) suffer from a semantic-spatial misalignment. While LLMs (Yang et al. 2024a; Shao et al. 2024) excels at decomposing abstract instructions into object lists, it lacks the intrinsic geometric intuition to model the strong conditional spatial dependencies between objects (*e.g.*, the canonical relative pose between a bed and a nightstand). In non-Manhattan environments, where spatial relations cannot be implicitly learned via axis-aligned patterns, this deficiency leads to

layouts that are physically valid but functionally incoherent. To bridge these gaps, we present *SPG-Layout*, a novel text-driven framework tailored for generating physically plausible indoor scenes within complex non-Manhattan environments.

To tackle the issue of spatially incoherent layouts, we propose a two-stage training paradigm empowered by *Spatial Prior Guidance*. Specifically, we align the LLM with structured scene representations and subsequently optimize the model using reinforcement learning. To ensure generation quality, we design verifiable rewards derived from the statistical distribution of non-Manhattan environments. Furthermore, to mitigate physical collisions, we introduce a *Hierarchical Layout Strategy* inspired by human interior design cognition. By adopting a coarse-to-fine workflow that prioritizes large-scale furniture before allocating smaller items to the remaining space, we effectively mitigate spatial conflicts and ensure physical plausibility, even in constrained geometries. Validating performance in non-Manhattan settings remains challenging due to data scarcity. To address this, we curated a novel dataset of 500 high-quality non-Manhattan scenes. We extracted irregular boundaries from publicly available professional floor plans and generated initial 3D layouts, which were subsequently polished via manual refinement to ensure quality. This dataset is then used to benchmark model performance in non-Manhattan environments. For completeness, we also conducted extensive experiments on standard Manhattan datasets. Empirical results demonstrate that our proposed *SPG-Layout* significantly outperforms the existing state-of-the-art baselines in both Manhattan and non-Manhattan environments, establishing itself as a versatile and robust framework for text-driven 3D indoor scene synthesis.

Our contributions are threefold: **First**, we propose *SPG-Layout*, the first text-driven framework specifically optimized for non-Manhattan indoor environments. By breaking the “Manhattan Assumption”, our approach enables physically plausible and semantically coherent 3D scene generation in complex architectural spaces with irregular boundaries and arbitrary angles. **Second**, we introduce a dual-optimization strategy that mirrors human design cognition: (i) *Spatial Prior Guidance (SPG)*, which integrates statistical distributions of object-boundary and object-object relationships into a reinforcement learning reward; and (ii) a *Hierarchical Layout Strategy (HLS)*, which prioritizes large-scale furniture to resolve spatial fragmentation and minimize physical collisions. **Third**, we propose the benchmark consisting of 500 diverse non-Manhattan environments to bridge the gap in existing datasets. Extensive evaluations demonstrate that *SPG-Layout* significantly outperforms current methods in both layout fidelity and violation metrics across Manhattan and non-Manhattan settings, establishing a robust baseline for future research.

2 Related Work

2.1 Indoor Scene Layout Generation

Early indoor scene layout generation relied on heuristic rules, procedural modeling, and optimization-based techniques (Qi et al. 2018; Weiss et al. 2018; Fisher et al. 2015; Purkait

et al. 2020), where handcrafted spatial constraints and expert knowledge were designed to produce functional and physically plausible layouts. With the emergence of deep learning, data-driven approaches gradually replaced manually designed rules. Representative methods include CNN-based scene priors (Wang et al. 2018), autoregressive transformer models (Ritchie, Wang, and Lin 2019; Wang, Yeshwanth, and Nießner 2021; Paschalidou et al. 2021; Sun et al. 2024b), and more recently diffusion-based approaches (Tang et al. 2024; Hu et al. 2024a; Wei et al. 2023; Maillard et al. 2024; Yang et al. 2024b). By learning object distributions from large-scale indoor scene datasets, these methods substantially improve layout realism and generation quality. Nevertheless, they primarily rely on learned spatial priors and predefined conditioning signals, making it difficult to flexibly synthesize scenes according to diverse user requirements.

2.2 Language-Guided Indoor Scene Generation

Recent advances in large language models (LLMs) have enabled indoor scene synthesis directly from natural language descriptions. Early work such as CLIP-Layout (?) explored language-conditioned layout generation using vision-language representations. Building upon instruction-following LLMs, subsequent methods—including LayoutGPT (Feng et al. 2023), LayoutVLM (Sun et al. 2024a), I-Design (Çelen et al. 2025), Holodeck (Yang et al. 2024d), LLPlace (Yang et al. 2024c), InstructScene (Lin and Mu 2024), SceneWeaver (Yang et al. 2025), Ctrl-Room (Fang et al. 2025), and ReSpace (Bucher and Armeni 2025)—significantly improve semantic controllability by allowing users to specify layout requirements through natural language instead of manually designing optimization objectives or spatial constraints. Despite these advances, existing methods are almost exclusively developed and evaluated on Manhattan-style environments, where room geometry can be approximated by axis-aligned boundaries.

2.3 Challenges of Non-Manhattan Scene Generation

Real-world indoor environments frequently deviate from the Manhattan-world assumption, exhibiting arbitrary wall orientations and irregular room boundaries. Such non-Manhattan geometries have been extensively studied in indoor layout estimation, floor-plan reconstruction, and scene understanding (Zou et al. 2018; Sun et al. 2019; Kalervo et al. 2019; Zheng et al. 2020), leading to increasingly accurate geometric representations of complex indoor spaces. However, these studies primarily focus on recovering room structures rather than generating object layouts conditioned on user intent. Consequently, although recent LLM-based scene synthesis methods achieve impressive language understanding and semantic reasoning capabilities, they generally lack explicit modeling of non-orthogonal spatial relationships and polygonal room geometries. Applying them directly to irregular floor plans often results in physically implausible object placements and inconsistent orientations. However, our method learns features under non-Manhattan layouts by constructing spatial priors, enabling text-driven scene synthesis to generalize to general non-Manhattan environments.

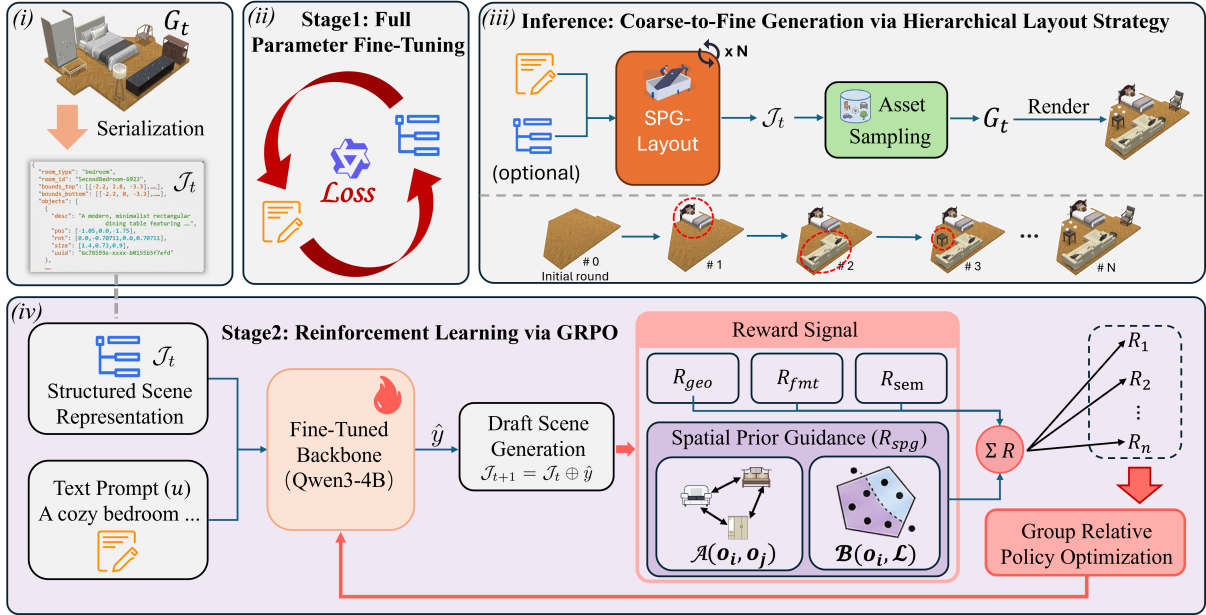


Figure 2: **Overview of the proposed SPG-Layout framework.** (i) Provides an intuitive comprehension of structured scene representation (Sec. 3.1). (ii) Structural alignment by full parameter fine-tuning (Sec. 4.3 stage 1). (iii) Inference Pipeline illustrates the hierarchical layout strategy for progressive generation (Sec. 4.4). (iv) Reinforcement Learning optimizes the model using a multi-objective reward function via GRPO (Sec. 4.3 stage 2).

3 Preliminaries and Problem Statement

3.1 Preliminaries

We represent a 3D indoor scene using a *Structured Scene Representation (SSR)*, which disentangles the scene into an architectural layout and a set of object instances.

Layout Definition. Let the room layout \mathcal{L} be defined by the ceiling and floor boundaries, each represented as an ordered sequence of vertices, $\mathcal{V}^{top} = (\mathbf{v}_1^{top}, \dots, \mathbf{v}_m^{top})$ and $\mathcal{V}^{bottom} = (\mathbf{v}_1^{bottom}, \dots, \mathbf{v}_m^{bottom})$, where $\mathbf{v}_i^{top}, \mathbf{v}_i^{bottom} \in \mathbb{R}^3$. Adjacent vertices in each sequence define the polygon edges, and the first and last vertices are connected to form closed polygons in Euclidean space. These boundaries specify the room envelope and impose structural constraints for object placement.

Object Parameterization. To support open-vocabulary synthesis, we represent each object o_i as a tuple that decouples semantics from geometry:

$$o_i = (d_i, \mathbf{s}_i, \mathbf{p}_i, \mathbf{q}_i), \quad (1)$$

where d_i denotes the natural language description (e.g., “a leather sofa”), and $\mathbf{s}_i \in \mathbb{R}^3$, $\mathbf{p}_i \in \mathbb{R}^3$, $\mathbf{q}_i \in \mathbb{R}^4$ correspond to the 3D scale, position, and rotation, respectively. This factorization enables asset-agnostic synthesis via cross-modal retrieval.

3.2 Problem Statement

We formulate text-driven indoor scene synthesis as a conditional sequence generation task. At generation step t , the

scene state is represented as $G_t = (\tau, \mathcal{L}, \mathcal{O}_t)$, where τ denotes the semantic room type inferred from the user prompt u , \mathcal{L} represents the geometric layout, and $\mathcal{O}_t = \{o_i\}_{i=1}^n$ is the set of instantiated objects.

To leverage the generative capabilities of LLMs, we introduce a serialization function $\mathcal{S} : \mathcal{G} \rightarrow \mathcal{J}$, which maps the structured scene state space \mathcal{G} into a discrete SSR sequence space \mathcal{J} . Given the user prompt u and the serialized context $\mathcal{J}_t = \mathcal{S}(G_t)$ of the current state, our objective is to generate a layout-compliant structural increment $\hat{y} \in \mathcal{J}$ by maximizing the conditional likelihood:

$$\hat{y} = \arg \max_{y \in \mathcal{J}} p_\theta(y | u, \mathcal{J}_t). \quad (2)$$

The SSR is then updated in the serialized space as $\mathcal{J}_{t+1} = \mathcal{J}_t \oplus \hat{y}$, where \oplus denotes the SSR update operator. The updated structured scene state G_{t+1} is subsequently sampled from \mathcal{J}_{t+1} , after which concrete assets are retrieved and instantiated to obtain the executable 3D scene. The generation process is initialized at $t = 0$ with $G_0 = (\tau(u), \mathcal{L}, \emptyset)$, whose serialized form is $\mathcal{J}_0 = \mathcal{S}(G_0)$.

4 Framework

This section details our 3D indoor scene synthesis framework (see Fig. 2). We first describe the non-Manhattan data generation pipeline (Sec. 4.1). Then, we introduce the Spatial Prior Guidance mechanism (Sec. 4.2) and the two-stage training process (Sec. 4.3). Finally, we present the hierarchical strategy used for inference in Sec. 4.4.

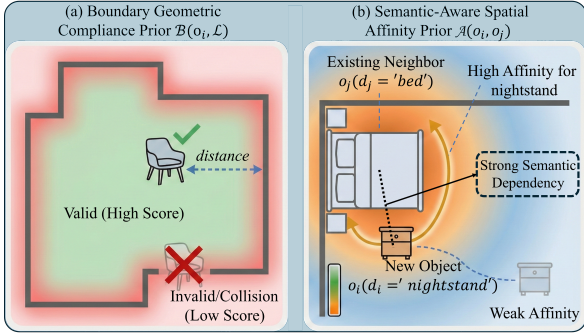


Figure 3: **Mechanism of Spatial Prior Guidance (SPG)**. SPG explicitly integrates geometric boundary priors and semantic co-occurrence affinities to provide computable reward signals for reinforcement learning-based scene generation.

4.1 Non-Manhattan Data Collection

To facilitate our research on non-Manhattan Environments, we present a semi-automated data generation pipeline, illustrated in Fig. 7, to construct a dataset of non-Manhattan 3D indoor scenes. Specifically, we first curate a large-scale collection of raw floor plan templates from web repositories and extract their geometric boundaries, formulated as \mathcal{L} . To populate these empty rooms, we utilize a model pre-trained on Manhattan datasets (specifically, the ReSpace (Bucher and Armeni 2025) model integrated with our HLS strategy) to synthesize coarse non-Manhattan scenes. Since direct transfer may introduce artifacts, we subsequently employ a manual refinement process where annotators manually adjust the pose and scale of objects to ensure physical plausibility and semantic coherence. This pipeline ultimately yields a curated dataset of 500 high-quality refined scenes. See more details in Sec. 8.

4.2 Spatial Prior Guidance

While LLMs excel at semantic decomposition—parsing user prompts into object tuples $\mathbf{o}_i = (d_i, \mathbf{s}_i, \mathbf{p}_i, \mathbf{q}_i)$ —they exhibit significant limitations in spatial positioning \mathbf{p}_i and geometric reasoning. Existing autoregressive approaches directly regress object parameters, effectively memorizing coordinate distributions from training data. In non-Manhattan environments with irregular boundaries \mathcal{L} , these memorized distributions fail to generalize: positions that are valid in Manhattan settings may fall outside the valid polygon, causing collisions or implausible placements. Moreover, without explicit spatial priors, the model lacks the inductive bias to capture conditional dependencies $P(\mathbf{o}_i | \mathbf{o}_j)$ between semantically affiliated objects (e.g., a nightstand adjacent to a bed) in irregular geometries.

To address these challenges, we introduce *Spatial Prior Guidance (SPG)*. Instead of relying solely on the textual likelihood, we explicitly model the statistical priors of object-boundary relationships and object-object affinities, as illustrated in Fig. 3. Formally, we quantify the SPG as a scoring function R_{spg} that evaluates the spatial validity of the gener-

ated position:

$$R_{\text{spg}}(\mathbf{o}_i, \mathcal{L}, \mathcal{O}_{<i}) = \alpha \cdot \mathcal{B}(\mathbf{o}_i, \mathcal{L}) + \beta \cdot \sum_{\mathbf{o}_j \in \mathcal{O}_{<i}} w_j \cdot \mathcal{A}(\mathbf{o}_i, \mathbf{o}_j), \quad (3)$$

where $\mathcal{B}(\cdot)$ measures the object-architecture prior consistency, and $\mathcal{A}(\cdot)$ calculates the semantic-aware spatial affinity between the current object and its neighbors in the previously generated set $\mathcal{O}_{<i}$. Sensitivity coefficients α and β balance the contribution of each prior. The weight w_j is computed via an attention mechanism:

$$w_j = \frac{\exp(\mathcal{A}(\mathbf{o}_i, \mathbf{o}_j)/\tau)}{\sum_{\mathbf{o}_k \in \mathcal{O}_{<i}} \exp(\mathcal{A}(\mathbf{o}_i, \mathbf{o}_k)/\tau)}, \quad (4)$$

where τ is a learnable temperature parameter. Unlike naive averaging, which dilutes the spatial signal with noise from weakly related objects, this attention-weighted aggregation dynamically assigns higher weights to semantically stronger spatial anchors (e.g., the bed as the primary anchor for a nightstand), while still retaining information from all previously placed objects. This formulation transforms abstract spatial constraints into a computable metric. R_{spg} serves as an intrinsic reward signal that guides policy optimization in the reinforcement learning stage. We emphasize that R_{spg} provides the model with directional guidance toward human-preferred spatial distributions rather than exposing ground-truth answers; combined with the KL divergence penalty in GRPO, this prevents reward hacking and ensures the model learns generalizable spatial reasoning rather than overfitting to specific evaluation criteria.

4.3 Two-Stage Training Strategy

We propose a two-stage training pipeline to adapt a general-purpose LLM for 3D scene layout generation. The first stage aligns the model to the SSR format via Supervised Fine-Tuning, and the second stage enforces geometric constraints via Reinforcement Learning with Group Relative Policy Optimization (GRPO). **Stage 1: Supervised Fine-Tuning for Structural Alignment.**

A key requirement for text-driven scene synthesis is adherence to the SSR format defined in Sec. 3.1. We fine-tune the Qwen3-4B backbone on SSR-3DFRONT (Bucher and Armeni 2025)—a structured version of 3D-FRONT (Fu et al. 2021). We use full-parameter fine-tuning rather than LoRA (Hu et al. 2022), as LoRA achieves only a 78% format success rate compared to 99% for full fine-tuning after training for 100 epochs. Such high format compliance is necessary for the RL stage to correctly parse and optimize object parameters.

Stage 2: Reinforcement Learning via GRPO.

While the first stage enables valid syntax generation, it does not enforce continuous physical constraints such as object intersections or boundary violations. We further optimize the SFT model using GRPO to improve geometric plausibility.

To balance geometric consistency, format compliance, semantic matching, and spatial reasoning, we employ a multi-

objective reward function, as defined in Eq. 5:

$$R_{total} = \begin{cases} R_{fmt}, & R_{fmt} \neq 1, \\ \gamma_1 R_{geo} + \gamma_2 R_{sem} \\ \quad + \frac{\gamma_3}{N} \sum_{i=1}^N R_{spg}, & \text{otherwise.} \end{cases} \quad (5)$$

where γ_i ($i \in \{1, 2, 3\}$) represents the weight coefficient for each reward component, and N denotes the number of objects in the synthesized scene. The specific definitions of each reward component are as follows:

Geometric Consistency Reward (R_{geo}). We design the geometric reward to enforce physical constraints by minimizing an energy-based cost. The *geometric energy* \mathcal{E}_{geo} measures the severity of boundary violations and object collisions:

$$\mathcal{E}_{geo} = \sum_i \underbrace{\|\mathbf{V}_i \odot (\mathbf{1} - \mathbf{V}_{env})\|_1}_{\text{Boundary Violation}} + \sum_{i < j} \underbrace{\|\mathbf{V}_i \odot \mathbf{V}_j\|_1}_{\text{Collision}}, \quad (6)$$

where \mathbf{V}_i denotes the voxelized grid of the i -th object, and \mathbf{V}_{env} represents the environment layout (with 1 indicating valid interior space). \odot denotes the Hadamard product, and $\|\cdot\|_1$ is the L_1 norm measuring the volume of overlap. The final reward is obtained by normalizing this energy via exponential normalization: $R_{geo} = \exp(-\mathcal{E}_{geo}/\sigma_{geo})$. This mapping ensures that collision-free layouts receive a reward approaching 1, while invalid configurations yield smooth penalties to facilitate gradient-based optimization.

Format Compliance Reward (R_{fmt}). To guarantee that the generated outputs constitute a valid Structured Scene Representation (SSR) as defined in Sec. 3.1, we impose a strict structural constraint. Let $\Phi(o_i)$ be a validation function that returns 1 if and only if the generated object o_i can be successfully parsed into the tuple $(d_i, \mathbf{s}_i, \mathbf{p}_i, \mathbf{q}_i)$ with correct dimensionality ($\mathbf{s}_i, \mathbf{p}_i \in \mathbb{R}^3, \mathbf{q}_i \in \mathbb{R}^4$). The reward is the average validity over N generated objects:

$$R_{fmt} = \frac{1}{N} \sum_{i=1}^N \Phi(o_i). \quad (7)$$

This ensures the model strictly adheres to the defined schema, preventing malformed outputs that would fail the subsequent rendering process.

Semantic Matching Reward (R_{sem}). We quantify semantic fidelity by measuring the recall of mandatory attribute keywords, complementing latent-space metrics. Let \mathcal{K} denote the set of keywords extracted from the user prompt (e.g., {"red", "leather"}), and \mathcal{W}_i be the set of tokens in the generated object description. The reward is defined as the average keyword coverage:

$$r_i = \frac{1}{|\mathcal{K}|} \sum_{w \in \mathcal{K}} \mathbb{I}[w \in \bigcup_i \mathcal{W}_i], \quad R_{sem} = \frac{1}{N} \sum_i r_i. \quad (8)$$

This metric explicitly penalizes the omission of fine-grained constraints, ensuring the synthesized scene textually aligns with specific user instructions. Note that, if $|\mathcal{K}| = 0$, this term is excluded from the overall reward.

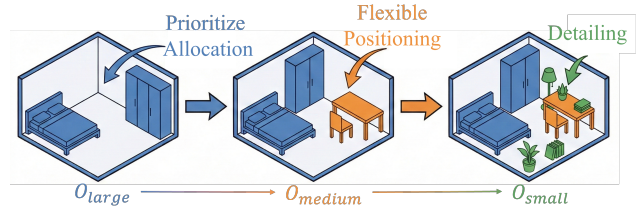


Figure 4: The Illustration of HLS.

4.4 Hierarchical Layout Strategy

While SPG-Layout excels in incremental object placement within existing scenes, text-driven 3D scene synthesis necessitates the ability to generate holistic scenes from scratch. In the absence of established spatial references, the unprioritized placement of smaller objects risks fragmenting the continuous free space. This fragmentation creates severe geometric constraints, often rendering the subsequent accommodation of larger structures infeasible due to collision conflicts. Conversely, prioritizing larger entities establishes a spatial backbone, ensuring sufficient allocation for dominant structures while allowing smaller items to be flexibly positioned within the remaining interstices.

Drawing inspiration from human cognitive strategies in interior design—where dominant furniture pieces (e.g., beds, sofas) are positioned prior to supplementary items (e.g., stools, side tables)—we introduce the Hierarchical Layout Strategy (HLS). Specifically, we categorize objects into three distinct tiers based on area occupancy: large (\mathcal{O}_{large} , $area > 1.2$), medium (\mathcal{O}_{medium} , $0.3 \leq area \leq 1.2$) and small (\mathcal{O}_{small} , $area < 0.3$). HLS strictly enforces a descending order of placement ($\mathcal{O}_{large} \rightarrow \mathcal{O}_{medium} \rightarrow \mathcal{O}_{small}$), prioritizing the localization of large objects before determining the coordinates for smaller entities (As shown in Fig. 4).

Furthermore, HLS is adapted as a dynamic conflict resolution mechanism during single-object addition. When the initial scene layout is suboptimal and leads to collisions between the SPG-Layout prediction and existing objects, HLS temporarily retracts all existing objects smaller than the new entity into a candidate pool. The system then re-optimizes the layout by placing all objects in the pool (including the new one) following the hierarchical size-descending protocol. This approach facilitates the seamless integration of new objects while maximally preserving the structural integrity and semantic consistency of the original scene.

5 Experiments

We evaluate SPG-Layout on two tasks in non-Manhattan environments: 1) **Single Object Addition**: inserting new objects into existing layouts via text instructions; 2) **Full Scene Synthesis**: generating complete layouts from text descriptions alone. We also benchmark against methods restricted to orthogonal geometries in standard Manhattan settings. Finally, we conduct ablation studies to validate each proposed module.

5.1 Experimental Setup

We evaluate on the 500 non-Manhattan scenes from Sec. 4.1, partitioned into ‘bed’ (252), ‘liv’ (148), and ‘all’ (500) splits

Table 1: **Quantitative comparison on layout generation.** We report results as *Single Object Addition / Full Scene Synthesis* tasks. Layout Violations metrics are multiplied by 10^3 for readability. \uparrow indicates higher is better, and \downarrow indicates lower is better. **Bold** indicates the best performance for each setting respectively. “n/a” denotes inapplicable metrics.

Category	Method	Layout Violations			Layout Fidelity			
		\downarrow OOB $\times 10^3$	\downarrow MBL $\times 10^3$	\downarrow VBL $\times 10^3$	\uparrow OOR(%)	\uparrow OAR(%)	\uparrow ATR(%)	\uparrow PMS(%)
Bed.	LayoutGPT (Feng et al. 2023)	850.91 / 2243.30	251.20 / 662.26	1102.11 / 2905.56	8.15 / 6.02	11.39 / 8.42	16.03 / 11.85	n/a / n/a
	LayoutVLM (Sun et al. 2024a)	192.22 / 506.76	193.58 / 510.36	385.80 / 1017.12	34.64 / 25.61	40.14 / 29.67	47.91 / 35.41	n/a / n/a
	InstructScene (Lin and Mu 2024)	338.22 / 891.68	414.73 / 1093.38	752.95 / 1985.06	17.16 / 12.69	25.36 / 18.74	32.55 / 24.06	n/a / n/a
	ATISS (Paschalidou et al. 2021)	237.7 / 523.2	156.7 / 330.8	394.4 / 853.2	33.13 / 23.87	41.54 / 29.78	56.78 / 34.90	52.00 / n/a
	MiDiffusion (Hu et al. 2024a)	158.0 / 422.3	114.1 / 298.8	272.2 / 721.1	36.87 / 28.78	47.89 / 35.94	61.52 / 39.02	50.00 / n/a
	ReSpace (Bucher and Armeni 2025)	53.22 / 261.5	11.17 / 167.2	64.39 / 428.7	58.32 / 60.69	74.01 / 71.81	89.68 / 77.38	91.00 / 87.00
	SPG-Layout (Ours)	1.56 / 29.30	1.63 / 30.39	3.19 / 59.69	63.64 / 62.81	79.42 / 75.71	88.71 / 81.57	91.00 / 89.00
Liv.	LayoutGPT (Feng et al. 2023)	724.85 / 1910.96	213.99 / 564.15	938.83 / 2475.10	8.48 / 6.27	11.86 / 8.77	16.68 / 12.33	n/a / n/a
	LayoutVLM (Sun et al. 2024a)	163.74 / 431.68	164.91 / 434.75	328.65 / 866.43	36.06 / 26.65	41.78 / 30.88	49.86 / 36.86	n/a / n/a
	InstructScene (Lin and Mu 2024)	288.12 / 759.58	353.29 / 931.40	641.41 / 1690.98	17.86 / 13.20	26.39 / 19.51	33.88 / 25.04	n/a / n/a
	ATISS (Paschalidou et al. 2021)	197.0 / 504.3	131.2 / 254.8	328.2 / 759.1	36.13 / 29.56	43.54 / 31.59	58.78 / 36.88	56.00 / n/a
	MiDiffusion (Hu et al. 2024a)	142.3 / 352.6	99.76 / 237.2	242.0 / 589.8	41.08 / 31.73	48.70 / 32.21	67.52 / 37.94	57.00 / n/a
	ReSpace (Bucher and Armeni 2025)	31.01 / 190.5	13.29 / 65.20	44.30 / 255.7	61.21 / 63.43	65.99 / 65.38	89.05 / 83.41	90.00 / 89.00
	SPG-Layout (Ours)	1.47 / 4.05	1.30 / 6.06	2.77 / 10.11	66.69 / 65.54	67.63 / 69.66	89.60 / 84.37	90.00 / 89.00
All	LayoutGPT (Feng et al. 2023)	787.88 / 2077.12	232.59 / 613.20	1020.47 / 2690.33	8.31 / 6.15	11.63 / 8.59	16.35 / 12.09	n/a / n/a
	LayoutVLM (Sun et al. 2024a)	177.98 / 469.22	179.25 / 472.55	357.23 / 941.77	35.35 / 26.13	40.96 / 30.28	48.89 / 36.13	n/a / n/a
	InstructScene (Lin and Mu 2024)	313.17 / 825.63	384.01 / 1012.39	697.18 / 1838.02	17.51 / 12.95	25.87 / 19.12	33.21 / 24.55	n/a / n/a
	ATISS (Paschalidou et al. 2021)	221.7 / 631.4	114.5 / 108.5	336.1 / 739.8	35.92 / 27.56	44.04 / 23.66	57.09 / 28.76	55.00 / n/a
	MiDiffusion (Hu et al. 2024a)	153.5 / 327.4	102.9 / 87.10	256.4 / 414.5	39.77 / 29.02	47.00 / 26.88	65.10 / 31.23	53.00 / n/a
	ReSpace (Bucher and Armeni 2025)	34.33 / 218.4	12.26 / 91.94	46.60 / 310.3	60.24 / 60.61	73.17 / 69.07	89.23 / 82.51	90.00 / 90.00
	SPG-Layout (Ours)	0.59 / 14.93	1.12 / 14.36	1.71 / 29.29	66.18 / 65.71	76.68 / 74.78	89.09 / 83.63	89.00 / 92.00

following ReSpace (Bucher and Armeni 2025). For Manhattan comparison, we sample an equivalent subset from SSR-3DFRONT (Bucher and Armeni 2025). We report Layout Violation metrics (OOB, MBL, VBL) and Layout Fidelity metrics (OOR, OAR, ATR, PMS), with definitions in Sec. 9. Independent SceneEval (Tam et al. 2026) results are in Sec. 13.1.

5.2 Main Results

The model is trained on SSR-3DFRONT (Bucher and Armeni 2025) for 110 epochs, comprising 100 epochs of supervised fine-tuning and 10 epochs of reinforcement learning. GRPO is adopted with a group size of 8, where $\alpha = 0.55$ and $\beta = 0.45$ in Eq. 3, and $\gamma_{1-3} = 0.3, 0.3, 0.4$ in Eq. 5.

Single Object Addition. Tab. 1 shows SPG-Layout outperforms baselines by a significant margin. In the ‘bedroom’ subset, OOB, MBL, and VBL are reduced by 51.66, 9.54, and 61.2, respectively. OOR and OAR improve by an average of 5.58 and 3.52 across all categories.

Full Scene Synthesis. Starting from an empty scene, the model must synthesize the entire layout from text alone. Tab. 1 demonstrates layout violation reductions of 86%, 96%, and 91% in the Bedroom, Living room, and All categories over the runner-up, while achieving SOTA fidelity. The attention-weighted SPG (Eq. 3) improves OOR from 63.39% to 65.71% in the All category compared to the averaging baseline, confirming that dynamically weighting spatial anchors yields more effective guidance. Qualitative results are shown in Fig. 6 and Fig. 5.

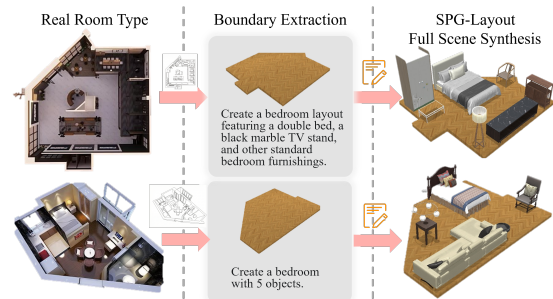


Figure 5: **Qualitative Results on non-Manhattan Dataset.** Given real-world room type, SPG-Layout generates complete scene layouts guided by specific user instructions.

5.3 Generalization Capacity and User Study

Generalization Capacity. To evaluate generalization, we test in standard Manhattan environments (Tab. 2). Results show that our method outperforms existing approaches in both non-Manhattan and conventional Manhattan settings.

User Study. We conducted a user study to evaluate perceptual quality in non-Manhattan scenes. We generated 100 comparison sets, each containing our method’s output alongside all baselines, presented in randomized and anonymized order. Twenty participants voted for the layout that best preserved spatial fidelity, object arrangement rationality, and consistency with the input description (Tab. 3).

Table 2: **Generalization results in conventional Manhattan environments.** \uparrow indicates higher is better, and \downarrow indicates lower is better. Layout Violations are multiplied by 10^3 for readability. **Bold** indicate the best performance.

Method	Layout Violations			Layout Fidelity			
	\downarrow OOB $\times 1e3$	\downarrow MBL $\times 1e3$	\downarrow VBL $\times 1e3$	\uparrow OOR(%)	\uparrow OAR(%)	\uparrow ATR(%)	\uparrow PMS(%)
LayoutGPT (Feng et al. 2023)	1199.7	84.21	1284.0	9.87	12.78	15.32	n/a
LayoutVLM (Sun et al. 2024a)	78.6	84.34	162.9	33.78	39.24	46.45	n/a
InstructScene (Lin and Mu 2024)	211.45	125.71	337.16	23.38	33.79	38.20	n/a
ATISS (Paschalidou et al. 2021)	412.75	250.8	663.55	26.87	32.78	37.85	n/a
Mi-Diff (Hu et al. 2024a)	422.3	298.8	721.1	35.06	41.37	44.98	n/a
ReSpace (Bucher and Armeni 2025)	88.8	124.60	213.4	69.61	77.29	78.32	72.00
SPG-Layout (Ours)	8.12	9.73	17.85	73.21	81.23	85.07	89.00

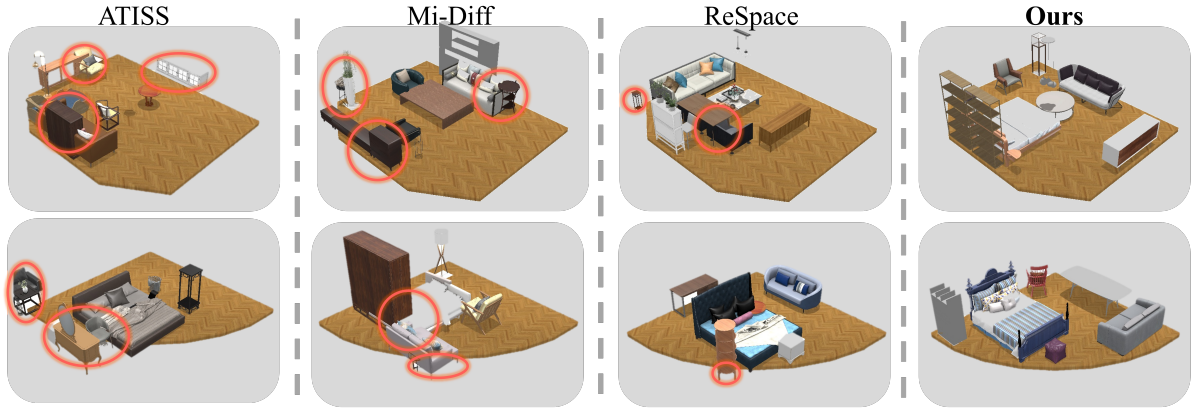


Figure 6: Qualitative results of layout generation in complex non-Manhattan environments compared to the existing methods. **Red circles** highlight instances of layout violations, such as object collisions or boundary penetrations.

Table 3: **User Study Results.** Twenty participants blindly voted for the best layout among anonymized results in each comparison set.

Method	LayoutGPT	LayoutVLM	InstructScene	ATISS	Mi-Diff	ReSpace	Ours
Votes	34	71	48	56	83	346	1362

5.4 Ablation Study

We report two aggregated metrics: **avg_LV** (mean of OOB, MBL, VBL) and **avg_LF** (mean of OOR, OAR, ATR, PMS). **Impact of Reward Signals.** As shown in the second row of Tab. 4, the SPG module improves layout quality and reduces violations. Without SPG, **avg_LF** of the three categories drops by 15.6%, 12.8% and 11.4%, and the average **avg_LV** increases by 50.74. The spatial prior of SPG enhances scene understanding and yields more reasonable layout coordinate predictions. Ablation on geometric reward R_{geo} (third row) reveals that removing R_{geo} slightly raises **avg_LV**. Its impact is negligible compared with HLS, indicating R_{geo} is not a core factor for mitigating layout violations.

Impact of Hierarchical Layout Strategy. As shown in the fourth row of Tab. 4, HLS is critical for mitigating layout violations. The full model reduces **avg_LV** by 100.73, 108.89, and 113.16 on the ‘bed’, ‘liv’, and ‘all’ splits compared with the model without HLS. This indicates that the hierarchical constraints of HLS prevent unreasonable placement of small

Table 4: **Ablation Study.**

Settings	avg_LV (\downarrow)			avg_LF (\uparrow)		
	bed	liv	all	bed	liv	all
baseline	285.78	170.47	206.86	74.22	75.31	75.54
SPG-Layout (w/o R_{spg})	88.09	54.77	75.41	65.18	67.24	69.45
SPG-Layout (w/o R_{geo})	102.77	86.09	78.76	76.64	75.08	77.89
SPG-Layout (w/o HLS)	140.52	115.63	132.68	73.25	74.81	76.39
SPG-Layout (full)	39.79	6.74	19.52	77.27	77.14	78.36

objects and effectively avoid collisions between objects.

6 Conclusion

In this paper, we present **SPG-Layout**, a novel text-driven framework for 3D indoor scene synthesis that effectively addresses the limitations of existing methods in handling non-Manhattan environments. By integrating *Spatial Prior Guidance* and *Hierarchical Layout Strategy* within a two-stage training framework, our approach achieves unprecedented advancements on complex non-Manhattan benchmark. Furthermore, comprehensive experiments reveal that SPG-Layout not only leads state-of-the-art baselines in general but also far exceeds the performance of existing methods on standard Manhattan Environments.

Appendix

This technical appendix provides additional details of metrics, implementation details of our method, as well as experimental results that are omitted from the main body of this paper due to the page limit.

7 Preliminary: Group Relative Policy Optimization (GRPO)

GRPO is a reinforcement learning algorithm for post-training large language models (LLMs). Compared with Proximal Policy Optimization (PPO), GRPO removes the need for an additional value (critic) network by estimating advantages through relative reward comparison within a group of sampled responses. This design significantly reduces computational and memory overhead while maintaining stable policy optimization.

Given an input prompt x , the old policy $\pi_{\theta_{\text{old}}}$ samples a group of G responses,

$$\{y_1, y_2, \dots, y_G\} \sim \pi_{\theta_{\text{old}}}(\cdot|x).$$

Each response is assigned a scalar reward r_i , and its advantage is computed by group-wise normalization:

$$A_i = \frac{r_i - \text{mean}(\{r_j\}_{j=1}^G)}{\text{std}(\{r_j\}_{j=1}^G) + \epsilon},$$

where ϵ is a small constant for numerical stability.

GRPO optimizes the policy using the following clipped surrogate objective:

$$\begin{aligned} \mathcal{L}_{\text{GRPO}}(\theta) = & \mathbb{E} \left[\frac{1}{G} \sum_{i=1}^G \left(\min \left(r_i(\theta) A_i, \text{clip}(r_i(\theta), 1 - \epsilon, 1 + \epsilon) A_i \right) \right. \right. \\ & \left. \left. - \beta D_{\text{KL}}(\pi_{\theta} \parallel \pi_{\text{ref}}) \right) \right], \end{aligned} \quad (9)$$

where

$$r_i(\theta) = \frac{\pi_{\theta}(y_i|x)}{\pi_{\theta_{\text{old}}}(y_i|x)}$$

denotes the importance sampling ratio, π_{ref} is the reference policy, ϵ is the clipping coefficient, and β controls the KL regularization strength. The clipped objective constrains the policy update, while the KL term prevents the optimized policy from deviating excessively from the reference model.

The above formulation is adopted as the reinforcement learning backbone in our method. Readers are referred to the original GRPO paper for a comprehensive derivation and theoretical analysis.

8 Details of Non-Manhattan Data Collection

Our dataset is collected in a copyright-respecting manner. All floor plans and related materials are obtained from publicly accessible sources under appropriate usage conditions, and we only use the information necessary for research purposes. We do not redistribute any proprietary raw content,

and all collected data are processed into derived representations (e.g., geometric layouts and annotations) that do not retain identifiable copyrighted elements.

Our prior extraction strategy is highly robust. Its main purpose is to prevent the model from simply memorizing absolute coordinates, and instead encourage it to learn the underlying distributions of object–object distances and object–wall distances in realistic indoor environments. Importantly, the priors are not extracted from the 500 test scenes. Instead, we estimate the priors using an additional set of 200 non-Manhattan scenes processed with the same refinement pipeline, combined with 100 manually refined scenes from conventional Manhattan environments. We adopt this mixed prior estimation strategy because relying solely on non-Manhattan data may reduce the model’s generalization ability. The total number of samples used for prior estimation is limited to 300 due to the substantial human cost of data refinement: even with a semi-automatic annotation workflow, polishing each scene still requires approximately 10–15 minutes of annotator effort. Therefore, we only use 300 high-quality scenes for prior extraction, which we believe best reflect real-world object arrangement patterns. As shown in Tab. 2, our method maintains strong generalization performance and still significantly outperforms existing approaches without re-estimating the priors.

9 Detailed Definitions of Evaluation Metrics

In this section, we provide the formal definitions and calculation details for the metrics used to evaluate our model. Let \mathcal{S} denote a generated scene containing a set of N objects, denoted as $\mathcal{O} = \{o_1, o_2, \dots, o_N\}$. Let \mathcal{R} represent the 3D space occupied by the room boundary.

9.1 Layout Violation Metrics

To strictly evaluate the physical plausibility of the synthesized scenes, we employ mesh-based voxelization to calculate violations with high precision, rather than relying on coarse bounding box approximations. We report the following three metrics:

- **Out-Of-Bounds (OOB):** This metric quantifies the volume of objects penetrating the room layout boundaries (e.g., floor, walls, ceiling). For each object o_i , we compute its voxelized mesh representation $\mathcal{V}(o_i)$. The OOB loss is defined as the total volume of object voxels lying outside the valid room space \mathcal{R} :

$$\mathcal{L}_{\text{OOB}} = \sum_{i=1}^N \text{Vol}(\mathcal{V}(o_i) \setminus \mathcal{R}), \quad (10)$$

where $\text{Vol}(\cdot)$ denotes the physical volume calculated from the voxel occupancy, and \setminus represents the set difference operation.

- **Mesh-Based Layout Loss (MBL):** This metric measures the severity of inter-object collisions. It is calculated as the sum of the intersection volumes between all pairs of distinct objects in the scene. Unlike bounding-box IoU,

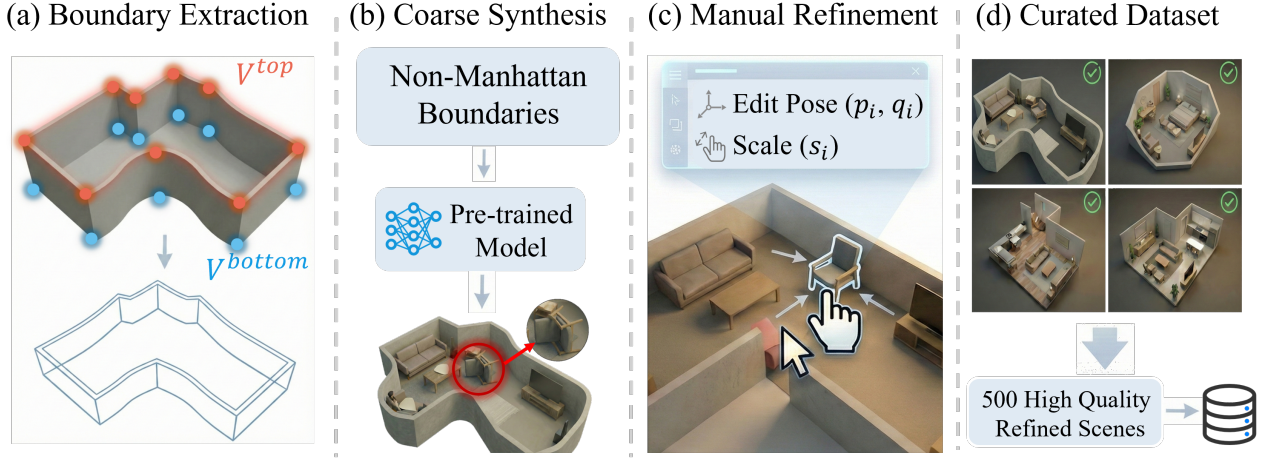


Figure 7: **Semi-Automated Data Generation Pipeline.** We extract geometric boundaries (a) and generate coarse scenes (b), followed by manual refinement of object attributes (c) to construct a curated dataset of 500 non-Manhattan scenes (d).

this metric accounts for the detailed geometry of the assets:

$$\mathcal{L}_{\text{MBL}} = \sum_{1 \leq i < j \leq N} \text{Vol}(\mathcal{V}(o_i) \cap \mathcal{V}(o_j)), \quad (11)$$

where \cap denotes the intersection of the voxelized meshes.

- **Voxelization-Based Loss (VBL):** VBL aggregates both boundary violations and inter-object collisions into a single measure of layout infeasibility:

$$\mathcal{L}_{\text{VBL}} = \mathcal{L}_{\text{OOB}} + \mathcal{L}_{\text{MBL}}. \quad (12)$$

In our reported tables, these metrics (\mathcal{L}_{OOB} , \mathcal{L}_{MBL} , \mathcal{L}_{VBL}) are typically scaled (e.g., $\times 10^3$) for better readability.

9.2 Layout Fidelity Metrics

To assess how well the generated layouts align with human design distributions and the input textual intent, we utilize the following four metrics:

- **Attribute Match (ATR):** ATR evaluates the semantic accuracy of the generated object categories. For a generated object o_i and its expected category from the prompt c_i^{gt} , the score is calculated as:

$$\text{ATR} = \frac{1}{N} \sum_{i=1}^N \mathbb{I}(\text{Cat}(o_i) = c_i^{gt}), \quad (13)$$

where $\mathbb{I}(\cdot)$ is the indicator function, and $\text{Cat}(\cdot)$ returns the semantic category of the object.

- **Object-Architecture Relationship (OAR):** This metric assesses the consistency of object placement relative to the room structure (walls). For each object o_i belonging to category c_i , we measure its Euclidean distance to the nearest wall, denoted as $d(o_i, \mathcal{L})$. Using the category-specific wall distance mean $\mu_{c_i}^w$ and standard deviation $\sigma_{c_i}^w$ derived from the human-refined dataset statistics, OAR is calculated as the ratio of objects that fall within the expected statistical range:

$$\text{OAR} = \frac{1}{N} \sum_{i=1}^N \mathbb{I}(|d(o_i, \mathcal{L}) - \mu_{c_i}^w| \leq \sigma_{c_i}^w), \quad (14)$$

where $\mathbb{I}(\cdot)$ is the indicator function. A higher OAR indicates that the spatial distribution of objects relative to the room boundaries mimics human design habits.

- **Object-Object Relationship (OOR):** This metric measures whether the pairwise spatial arrangements between objects follow the learned prior distribution of the dataset. For any pair of objects (o_i, o_j) with semantic categories (c_i, c_j) , let $\text{dist}(o_i, o_j)$ be the distance between their centers. Let \mathcal{P} be the set of all unique pairs in the scene, where $|\mathcal{P}| = \frac{N(N-1)}{2}$. The OOR score is defined as:

$$\text{OOR} = \frac{1}{|\mathcal{P}|} \sum_{(o_i, o_j) \in \mathcal{P}} \mathbb{I}(|\text{dist}(o_i, o_j) - \mu_{c_i, c_j}^p| \leq \sigma_{c_i, c_j}^p), \quad (15)$$

where μ_{c_i, c_j}^p and σ_{c_i, c_j}^p represent the mean and standard deviation of the pairwise distance for the category combination (c_i, c_j) as recorded in the statistical priors. This metric quantifies the plausibility of functional groupings, such as the typical proximity between a bed and a nightstand.

- **Prompt-Matching Score (PMS):** PMS quantifies the instruction-following capability by measuring the recall of words from the input prompt found in the description of the generated 3D asset. For a given input prompt p_i and the description d_i of the generated asset, the score is defined as:

$$\text{PMS}(p_i, d_i) = \frac{1}{|p_i|} \sum_{w_j \in p_i} \mathbb{I}_{w_j \in d_i}, \quad (16)$$

where w_j represents the j -th word in the prompt p_i , $|p_i|$ denotes the total word count of the prompt, and $\mathbb{I}_{\text{condition}}$ is the indicator function that equals 1 if the word w_j is present in the asset description d_i , and 0 otherwise.

10 The Detailed Implementation of Spatial Prior Guidance

In this section, we provide a detailed and reproducible description of how the **Spatial Prior Guidance (SPG)** module is implemented, including (i) how the statistical spatial priors are computed from human-refined scenes, and (ii) how these priors are instantiated as a computable reward to guide layout generation.

10.1 Overview and Notation

Given a generated scene \mathcal{S} containing N objects $\mathcal{O} = \{o_1, \dots, o_N\}$ and a room layout boundary \mathcal{L} , SPG introduces two types of priors:

- **Object-Architecture Prior:** category-dependent wall distance statistics (μ_c^w, σ_c^w) .
- **Object-Object Prior:** category-pair-dependent relative distance statistics $(\mu_{c_i, c_j}^p, \sigma_{c_i, c_j}^p)$.

These priors are estimated **offline** from the human-refined dataset, which exhibits a distribution more aligned with real-world scenarios, and are subsequently used during training to provide a dense reward signal that biases the model toward spatially plausible configurations.

10.2 Estimating Object-Architecture Priors

We first estimate the object-architecture priors used for evaluating and guiding **Object-Architecture Relationship (OAR)**. For each object o_i with semantic category c_i , we compute its Euclidean distance to the nearest wall in the room layout \mathcal{L} :

$$d(o_i, \mathcal{L}). \quad (17)$$

We then collect all wall-distance samples for each category c :

$$\mathcal{D}_c^w = \{d(o_i, \mathcal{L}) \mid \text{Cat}(o_i) = c\}. \quad (18)$$

Finally, we compute the category-wise mean and standard deviation:

$$\begin{aligned} \mu_c^w &= \frac{1}{|\mathcal{D}_c^w|} \sum_{d \in \mathcal{D}_c^w} d, \\ \sigma_c^w &= \sqrt{\frac{1}{|\mathcal{D}_c^w| - 1} \sum_{d \in \mathcal{D}_c^w} (d - \mu_c^w)^2}. \end{aligned} \quad (19)$$

These statistics capture human design preferences regarding object placements relative to architectural boundaries (e.g., beds and cabinets are often placed close to walls).

10.3 Estimating Object-Object Priors

We next estimate the object-object priors used for evaluating and guiding **Object-Object Relationship (OOR)**. For any object pair (o_i, o_j) with categories (c_i, c_j) , we compute their pairwise center distance:

$$\text{dist}(o_i, o_j). \quad (20)$$

We aggregate distances for each category pair (c_i, c_j) :

$$\mathcal{D}_{c_i, c_j}^p = \left\{ \text{dist}(o_i, o_j) \mid \begin{aligned} &\text{Cat}(o_i) = c_i, \\ &\text{Cat}(o_j) = c_j, i < j \end{aligned} \right\}. \quad (21)$$

Then, we compute the mean and standard deviation:

$$\begin{aligned} \mu_{c_i, c_j}^p &= \frac{1}{|\mathcal{D}_{c_i, c_j}^p|} \sum_{d \in \mathcal{D}_{c_i, c_j}^p} d, \\ \sigma_{c_i, c_j}^p &= \sqrt{\frac{1}{|\mathcal{D}_{c_i, c_j}^p| - 1} \sum_{d \in \mathcal{D}_{c_i, c_j}^p} (d - \mu_{c_i, c_j}^p)^2}. \end{aligned} \quad (22)$$

These statistics reflect typical functional groupings in indoor scenes, such as the expected proximity between a bed and a nightstand.

10.4 Instantiating $B(\cdot)$ and $A(\cdot)$ in SPG

Given a scene \mathcal{S} and an object o_i with category c_i , SPG introduces two components modeled as Gaussian kernels:

Object-Architecture Term $B(\cdot)$. The term $B(\cdot)$ quantifies the consistency of an object’s placement with the category-specific wall distance distribution. It is formulated as a Gaussian function:

$$B(o_i, \mathcal{L}) = \exp\left(-\frac{(d(o_i, \mathcal{L}) - \mu_{c_i}^w)^2}{2(\sigma_{c_i}^w)^2}\right). \quad (23)$$

Object-Object Term $A(\cdot)$. The term $A(\cdot)$ measures how well the relative distance between two objects conforms to the learned category-pair distribution:

$$A(o_i, o_j) = \exp\left(-\frac{(\text{dist}(o_i, o_j) - \mu_{c_i, c_j}^p)^2}{2(\sigma_{c_i, c_j}^p)^2}\right). \quad (24)$$

10.5 Discussion: Why SPG Improves OOR/OAR and Alleviates Collisions

Improving OOR/OAR. By construction, SPG directly optimizes the same statistical consistency criteria used by OOR and OAR. Therefore, maximizing \mathcal{R}_{SPG} encourages the model to generate layouts that lie within the high-probability regions of human-refined spatial distributions, leading to higher OOR and OAR scores.

Alleviating Collisions. Although SPG does not explicitly compute mesh intersections, it implicitly discourages object collisions through the object-object prior. In particular, when two objects overlap, their pairwise distance $\text{dist}(o_i, o_j)$ tends to be abnormally small and thus deviates from the learned mean μ_{c_i, c_j}^p for most functional category pairs. As a result, such configurations are assigned low \mathcal{R}_{SPG} , making them unlikely under the SPG-guided generation distribution. This explains why SPG can reduce collision frequency in practice, even without explicitly using voxel-based collision penalties. We emphasize that SPG serves as a *statistical* plausibility prior rather than a hard feasibility constraint. Thus, while SPG improves spatial rationality and reduces violations, strict collision-free guarantees require complementary geometric constraints, which are addressed by other components of the full framework.

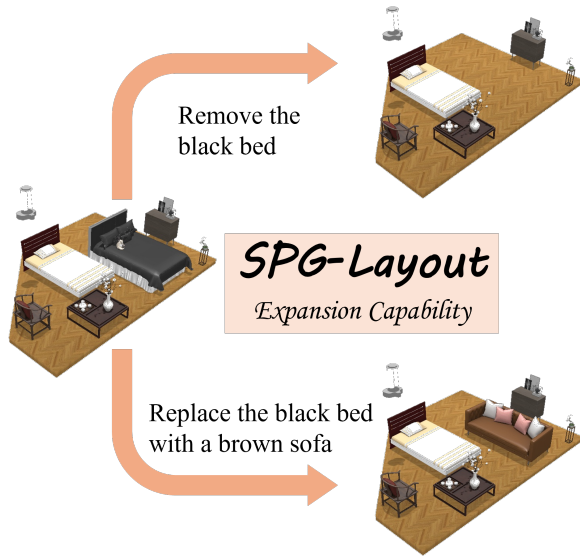


Figure 8: Expansion Capability of SPG-Layout.

11 Expansion Capability of Our framework

Leveraging Structured Scene Representation (SSR), our framework goes beyond scene synthesis and naturally supports object-level scene editing, including removal and replacement of existing entities. Under the explicit, object-centric SSR formulation, object removal becomes a straightforward and interpretable procedure. Specifically, we first enumerate and inspect the set of instantiated objects in the current scene. We then employ a zero-shot large language model (LLM) to parse the user instruction and identify the target object category or entity to be removed. Next, we perform semantic matching between the extracted target description and the existing object candidates using CLIP-based similarity, and eliminate the most semantically aligned object from the SSR. Because subsequent 3D asset retrieval and scene rendering are conditioned on the updated SSR, the removed object is consistently absent from the regenerated scene.

Similarly, object replacement can be formulated as a composition of removal followed by insertion: we first remove the original object using the above strategy, and then introduce the requested new object into the SSR, triggering the corresponding asset retrieval and rendering steps. Fig. 8 provides qualitative demonstrations of our framework on both remove and replace operations.

12 3D Asset Sampling

We retrieve 3D assets using a stochastic sampling process that balances semantic alignment and geometric fit. For a generated object o_i with description d_i and target scale s_i , we assign a selection score to each candidate mesh m_j in the asset library. The scoring function is defined as:

$$\text{Score}(m_j) = \lambda \cdot \text{sim}_{\text{sem}}(d_i, d_j) + (1 - \lambda) \cdot \text{sim}_{\text{geo}}(s_i, s_j). \quad (25)$$

where d_j and s_j denote the textual description and spatial dimensions of the candidate mesh m_j , respectively.

Specifically, the semantic similarity sim_{sem} is computed via the dot product of L2-normalized SigLIP embeddings. The geometric similarity sim_{geo} is calculated using a Gaussian kernel based on the Euclidean distance of 3D bounding box dimensions:

$$\text{sim}_{\text{geo}}(s_i, s_j) = \exp\left(-\frac{\|s_i - s_j\|_2^2}{2\sigma^2}\right), \quad (26)$$

where $\|\cdot\|_2$ denotes the L_2 norm. The final asset is selected via nucleus (top- p) sampling over the temperature-scaled softmax distribution derived from these scores. In line with the reference implementation, we set the weighting parameter $\lambda = 0.5$ to give equal importance to text description and spatial dimensions during retrieval.

13 Additional Experimental Results

13.1 Independent Evaluation with SceneEval Metrics

To address potential concerns about reward-metric circularity, we additionally evaluate our method using the independent metrics from SceneEval (?), which defines evaluation criteria independently of our reward design. As shown in Tab. 5, SPG-Layout consistently outperforms baselines across all independent metrics, confirming that our improvements reflect genuine layout quality rather than overfitting to the reward formulation.

Table 5: Independent evaluation using SceneEval metrics on Full Scene Synthesis (non-Manhattan, ‘all’ split).

Method	CNT \uparrow	ATR \uparrow	COL $_{ob}\downarrow$	SUP \uparrow	NAV \uparrow	OOB \downarrow
ATISS	10.72	7.29	56.27	82.77	78.12	31.86
MiDiffusion	12.85	11.32	43.78	88.58	88.96	18.97
ReSpace	65.81	38.49	2.37	98.32	98.71	0.16
SPG-Layout	82.33	55.76	0.24	99.23	99.40	0.03

13.2 Failure Cases

Collisions and out-of-bound placements are very rare in SPG-Layout and generally occur only when scenes contain an excessive number of objects. The majority of current failure cases relate to functional failures, particularly the orientation of small objects. We hypothesize that large objects typically have more distinctive features and stronger spatial relationships with other objects, making their distributions easier for the network to capture. In contrast, small objects are more numerous and span more diverse categories, making it harder for the model to learn sufficiently discriminative features. Failure case visualizations are available at Fig. 9.

13.3 Additional Qualitative Results

More visualization results are provided in this section, including additional visualization results generated by SPG-Layout (Fig. 10), as well as stacked scenes shown in Fig. 11.

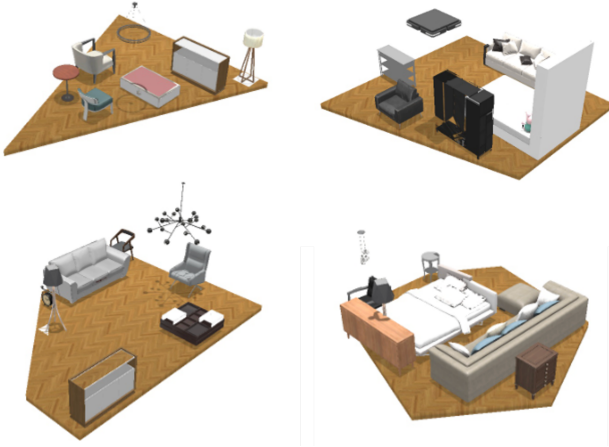


Figure 9: **Failure Cases.** Although no collisions occur, the generated layout severely deviates from human aesthetics, with cluttered and disorganized furniture arrangements.

13.4 Additional Ablation Study

To explore the impact of different aggregation operators in the SPG module, we conduct ablation experiments on the full scene synthesis task. The quantitative results are summarized in Table 6. We take two widely used aggregation strategies, Mean and Max, as baselines, and compare them with our proposed attention-based aggregation operator. Two evaluation metrics are adopted in our work: avg_LV (lower is better) and avg_LF (higher is better). We report the performance on bedroom (bed), living room (liv) and all scenes separately.

As shown in the table, Max aggregation achieves marginal improvements over Mean aggregation on most metrics, while it obtains slightly worse avg_LV results on the bedroom scene. However, both simple aggregation methods cannot fully model complex feature interactions. By contrast, our attention-based aggregation achieves competitive performance and obtains the optimal results on liv and all scenes in terms of avg_LV . Specifically, our method achieves avg_LV values of 39.79, 6.74 and 19.52 for bed, liv and all scenes, respectively, reaching the lowest avg_LV on living room and overall scenes. Meanwhile, our approach obtains the highest avg_LF score of 77.14 on the living room, with avg_LF scores of 77.27 and 78.36 for bedroom and all scenes correspondingly.

The above results indicate that static aggregation operations like Mean and Max fail to capture the importance of different features. Benefiting from adaptive weight assignment, the attention mechanism can effectively fuse multi-source features and model latent dependencies. This clearly verifies the rationality and effectiveness of our designed aggregation operator for full scene synthesis.

Limitations

Although SPG-Layout achieves strong performance across diverse indoor environments, it still has several limitations. Its reliance on spatial priors learned from 300 scenes may

Table 6: **Ablation of aggregation operators in SPG (Full Scene Synthesis).**

Aggregation	avg_LV (\downarrow)			avg_LF (\uparrow)		
	bed	liv	all	bed	liv	all
Mean	35.62	9.35	20.32	79.34	76.21	78.11
Max	35.77	8.63	19.82	79.89	76.36	78.62
Attention (Ours)	39.79	6.74	19.52	77.27	77.14	78.36

limit generalization to long-tail object categories. During single-object editing, HLS may introduce unintended global rearrangements when no collision-free insertion exists. In addition, fine-grained orientation remains challenging, especially for asymmetric or small objects, leading to occasional functional failures. Finally, the voxel-based geometric reward improves physical plausibility but incurs substantial computational overhead, reducing training efficiency.



Figure 10: More Visualizations.



Figure 11: Stacked Cases.

References

- Aguina-Kang, R.; Gumin, M.; Han, D. H.; Morris, S.; Yoo, S. J.; Ganeshan, A.; Jones, R. K.; Wei, Q. A.; Fu, K.; and Ritchie, D. 2024. Open-universe indoor scene generation using llm program synthesis and uncurated object databases. *arXiv preprint arXiv:2403.09675*.
- Bucher, M. J.; and Armeni, I. 2025. ReSpace: Text-Driven 3D Scene Synthesis and Editing with Preference Alignment. *arXiv preprint arXiv:2506.02459*.
- Celen, A.; Han, G.; Schindler, K.; Van Gool, L.; Armeni, I.; Obukhov, A.; and Wang, X. 2024. I-Design: Personalized LLM interior designer. In *Proceedings of the European Conference on Computer Vision (ECCV)*, 217–234.
- Fang, C.; Dong, Y.; Luo, K.; Hu, X.; Shrestha, R.; and Tan, P. 2025. Ctrl-Room: Controllable Text-to-3D Room Meshes Generation with Layout Constraints. In *Proceedings of the International Conference on 3D Vision (3DV)*, 692–701. IEEE.
- Feng, W.; Zhou, H.; Liao, J.; Cheng, L.; and Zhou, W. 2025. CasaGPT: cuboid arrangement and scene assembly for interior design. In *Proceedings of the Computer Vision and Pattern Recognition Conference*, 29173–29182.
- Feng, W.; Zhu, W.; Fu, T.-j.; Jampani, V.; Akula, A.; He, X.; Basu, S.; Wang, X. E.; and Wang, W. Y. 2023. Layoutgpt: Compositional visual planning and generation with large language models. *Advances in Neural Information Processing Systems*, 36: 18225–18250.
- Fisher, M.; Savva, M.; Hanrahan, P.; and Nießner, M. 2015. Activity-Centric Scene Synthesis for Functional 3D Scene Modeling. *ACM Transactions on Graphics (TOG)*, 34(6): 179:1–179:13.
- Fu, H.; Cai, B.; Gao, L.; Zhang, L.-X.; Wang, J.; Li, C.; Zeng, Q.; Sun, C.; Jia, R.; Zhao, B.; et al. 2021. 3d-front: 3d furnished rooms with layouts and semantics. In *Proceedings of the IEEE/CVF International Conference on Computer Vision*, 10933–10942.
- Fu, R.; Wen, Z.; Liu, Z.; and Sridhar, S. 2024. AnyHome: Open-vocabulary generation of structured and textured 3D homes. In *Proceedings of the European Conference on Computer Vision (ECCV)*, 52–70.
- Hao, X.; Zhou, L.; Huang, Z.; Hou, Z.; Tang, Y.; Zhang, L.; Li, G.; Lu, Z.; Ren, S.; Meng, X.; et al. 2025. MiMo-Embodied: X-Embodied Foundation Model Technical Report. *arXiv preprint arXiv:2511.16518*.
- Hu, E. J.; Shen, Y.; Wallis, P.; Allen-Zhu, Z.; Li, Y.; Wang, S.; Wang, L.; Chen, W.; et al. 2022. Lora: Low-rank adaptation of large language models. *ICLR*, 1(2): 3.
- Hu, S.; Arroyo, D. M.; Debats, S.; Manhardt, F.; Carlone, L.; and Tombari, F. 2024a. Mixed Diffusion for 3D Indoor Scene Synthesis. *arXiv preprint arXiv:2405.21066*.
- Hu, Z.; Iscen, A.; Jain, A.; Kipf, T.; Yue, Y.; Ross, D. A.; Schmid, C.; and Fathi, A. 2024b. SceneCraft: An LLM Agent for Synthesizing 3D Scenes as Blender Code. In *Proceedings of the International Conference on Machine Learning (ICML)*, volume 235, 19252–19282.
- Kalervo, A.; Ylioinas, J.; Häikiö, M.; Karhu, A.; and Kannala, J. 2019. CubiCasa5K: A Dataset and an Improved Multi-Task Model for Floorplan Image Analysis. In *Proceedings of the IEEE/CVF International Conference on Computer Vision Workshops (ICCVW)*.
- Lin, C.; and Mu, Y. 2024. Instructscene: Instruction-driven 3d indoor scene synthesis with semantic graph prior. *arXiv preprint arXiv:2402.04717*.
- Littlefair, G.; Dutt, N. S.; and Mitra, N. J. 2025. FlairGPT: Repurposing LLMs for interior designs. In *Computer Graphics Forum*, e70036.
- Maillard, L.; Sereyjol-Garros, N.; Durand, T.; and Ovsjanikov, M. 2024. Debara: Denoising-based 3d room arrangement generation. *Advances in Neural Information Processing Systems*, 37: 109202–109232.
- Paschalidou, D.; Kar, A.; Shugrina, M.; Kreis, K.; Geiger, A.; and Fidler, S. 2021. Atiss: Autoregressive transformers for indoor scene synthesis. *Advances in Neural Information Processing Systems*, 34: 12013–12026.
- Purkait, P.; Zach, C.; Chin, T.-J.; and Reid, I. 2020. Flexible Indoor Scene Synthesis Based on Multi-object Particle Swarm Intelligence Optimization and User Intentions with 3D Gesture. *Computers & Graphics*, 93: 1–12.
- Qi, S.; Zhu, Y.; Huang, S.; Jiang, C.; and Zhu, S. 2018. Human-Centric Indoor Scene Synthesis Using Stochastic Grammar. In *Proceedings of the IEEE/CVF Conference on Computer Vision and Pattern Recognition (CVPR)*, 5899–5908.
- Ritchie, D.; Wang, K.; and Lin, Y.-a. 2019. Fast and flexible indoor scene synthesis via deep convolutional generative models. In *Proceedings of the IEEE/CVF conference on computer vision and pattern recognition*, 6182–6190.
- Shao, Z.; Wang, P.; Zhu, Q.; Xu, R.; Song, J.; Bi, X.; Zhang, H.; Zhang, M.; Li, Y.; Wu, Y.; et al. 2024. Deepseekmath: Pushing the limits of mathematical reasoning in open language models. *arXiv preprint arXiv:2402.03300*.
- Song, Z.; Ouyang, G.; Fang, M.; Na, H.; Shi, Z.; Chen, Z.; Yujie, F.; Zhang, Z.; Jiang, S.; Fang, M.; et al. 2025. Hazards in daily life? enabling robots to proactively detect and resolve anomalies. In *Proceedings of the 2025 Conference of the Nations of the Americas Chapter of the Association for Computational Linguistics: Human Language Technologies (Volume 1: Long Papers)*, 7399–7415.
- Sun, C.; Hsiao, C.; Sun, M.; and Chen, H. 2019. HorizonNet: Learning Room Layout with 1D Representation and Pano Stretch Data Augmentation. In *Proceedings of the IEEE/CVF Conference on Computer Vision and Pattern Recognition (CVPR)*, 1047–1056.
- Sun, F.-Y.; Liu, W.; Gu, S.; Lim, D.; Bhat, G.; Tombari, F.; Li, M.; Haber, N.; and Wu, J. 2024a. LayoutVLM: Differentiable Optimization of 3D Layout via Vision-Language Models. *arXiv preprint arXiv:2412.02193*.
- Sun, Q.; Zhou, H.; Zhou, W.; Li, L.; and Li, H. 2024b. Forest2seq: Revitalizing order prior for sequential indoor scene synthesis. In *European Conference on Computer Vision*, 251–268.

- Tam, H. I. I.; Pun, H. I. D.; Wang, A. T.; Chang, A. X.; and Savva, M. 2026. SceneEval: Evaluating Semantic Coherence in Text-Conditioned 3D Indoor Scene Synthesis. In *Proceedings of the IEEE/CVF Winter Conference on Applications of Computer Vision (WACV)*.
- Tang, J.; Nie, Y.; Markhasin, L.; Dai, A.; Thies, J.; and Nießner, M. 2024. Diffuscene: Denoising diffusion models for generative indoor scene synthesis. In *Proceedings of the IEEE/CVF conference on computer vision and pattern recognition*, 20507–20518.
- Wang, C.; Zhong, H.; Chai, M.; He, M.; Chen, D.; and Liao, J. 2024. Chat2Layout: Interactive 3D Furniture Layout with a Multimodal LLM. *IEEE transactions on visualization and computer graphics*, PP.
- Wang, K.; Savva, M.; Chang, A. X.; and Ritchie, D. 2018. Deep convolutional priors for indoor scene synthesis. *ACM Transactions on Graphics (TOG)*, 37(4): 1–14.
- Wang, X.; Yeshwanth, C.; and Nießner, M. 2021. Sceneformer: Indoor scene generation with transformers. In *2021 International Conference on 3D Vision (3DV)*, 106–115. IEEE.
- Wang, Y.; Xian, Z.; Chen, F.; Wang, T.-H.; Wang, Y.; Fragkiadaki, K.; Erickson, Z.; Held, D.; and Gan, C. 2023. Robogen: Towards unleashing infinite data for automated robot learning via generative simulation. *arXiv preprint arXiv:2311.01455*.
- Wei, Q. A.; Ding, S.; Park, J. J.; Sajnani, R.; Poulenard, A.; Sridhar, S.; and Guibas, L. 2023. Lego-net: Learning regular rearrangements of objects in rooms. In *Proceedings of the IEEE/CVF Conference on Computer Vision and Pattern Recognition*, 19037–19047.
- Weiss, T.; Litteneker, A.; Duncan, N.; Nakada, M.; Jiang, C.; Yu, L.-F.; and Terzopoulos, D. 2018. Fast and scalable position-based layout synthesis. *IEEE Transactions on Visualization and Computer Graphics*, 25(12): 3231–3243.
- Xia, X.; Zhang, D.; Liao, Z.; Hou, Z.; Sun, T.; Li, J.; Fu, L.; and Dong, Y. 2025. SceneGenAgent: Precise Industrial Scene Generation with Coding Agent. In *Proceedings of the 63rd Annual Meeting of the Association for Computational Linguistics*, 17847–17875.
- Yang, A.; Yang, B.; Zhang, B.; Hui, B.; Zheng, B.; Yu, B.; Li, C.; Liu, D.; Huang, F.; Wei, H.; et al. 2024a. Qwen2. 5 technical report. *arXiv preprint arXiv:2412.15115*.
- Yang, Y.; Jia, B.; Zhang, S.; and Huang, S. 2025. SceneWeaver: All-in-One 3D Scene Synthesis with an Extensible and Self-Reflective Agent. *arXiv preprint arXiv:2509.20414*.
- Yang, Y.; Jia, B.; Zhi, P.; and Huang, S. 2024b. Physcene: Physically interactable 3d scene synthesis for embodied ai. In *Proceedings of the IEEE/CVF Conference on Computer Vision and Pattern Recognition*, 16262–16272.
- Yang, Y.; Lu, J.; Zhao, Z.; Luo, Z.; Yu, J. J.; Sanchez, V.; and Zheng, F. 2024c. Llplace: The 3d indoor scene layout generation and editing via large language model. *arXiv preprint arXiv:2406.03866*.
- Yang, Y.; Sun, F.-Y.; Weihs, L.; VanderBilt, E.; Herrasti, A.; Han, W.; Wu, J.; Haber, N.; Krishna, R.; Liu, L.; et al. 2024d. Holodeck: Language guided generation of 3d embodied ai environments. In *Proceedings of the IEEE/CVF Conference on Computer Vision and Pattern Recognition*, 16227–16237.
- Zhai, G.; Örnek, E. P.; Chen, D. Z.; Liao, R.; Di, Y.; Navab, N.; Tombari, F.; and Busam, B. 2024. Echoscene: Indoor scene generation via information echo over scene graph diffusion. In *European Conference on Computer Vision*, 167–184. Springer.
- Zheng, J.; Zhang, J.; Li, J.; Tang, R.; Gao, S.; and Zhou, Z. 2020. Structured3d: A large photo-realistic dataset for structured 3d modeling. In *European Conference on Computer Vision*, 519–535.
- Zou, C.; Colburn, A.; Shan, Q.; and Hoiem, D. 2018. LayoutNet: Reconstructing the 3D Room Layout from a Single RGB Image. In *Proceedings of the IEEE/CVF Conference on Computer Vision and Pattern Recognition (CVPR)*, 2051–2059.
- Çelen, A.; Han, G.; Schindler, K.; Gool, L. V.; Armeni, I.; Obukhov, A.; and Wang, X. 2025. I-Design: Personalized LLM Interior Designer. In *Computer Vision – ECCV 2024 Workshops*, Lecture Notes in Computer Science (LNCS), 217–234. Springer.